



Depression of direct exchange couplings in metallic glasses: A comparative study of critical and electronic behavior in $Gd_6Co_{4.85}$ intermetallic compound and metallic glass

Guoming Cui^a, Xin Li^{b,c}, Guangcun Shan^{b,d,**}, Haibin Gao^d, Kam Wa Wong^e, Jiliang Zhang^{f,*}

^a Department of Materials Science and Engineering, Henan Institute of Technology, Xinxiang, 453003, China

^b School of Instrument Science and Opto-electronics Engineering & Institute of Quantum Sensing, Beihang University, Beijing, 100083, China

^c Department of Materials Science and Engineering, City University of Hong Kong, Kowloon, Hong Kong, China

^d Institute of Experimental Physics, Saarland University, Saarbrücken, 66123, Germany

^e Department of Physics, City University of Hong Kong, Kowloon, Hong Kong, China

^f Department of Materials Science and Engineering, Korea University, Seoul, 04841, Republic of Korea

ARTICLE INFO

Keywords:

Intermetallics
Metallic glass
Electronic structure
Magnetic properties

ABSTRACT

Gd-based metallic glasses enable a wider exploration for excellent magnetocaloric materials due to no requirement of compositional stoichiometry, but these metallic glasses generally show a lower ordering temperature compared with corresponding intermetallic compounds. In this paper, critical behaviors for magnetic transitions in both $Gd_6Co_{4.85}$ intermetallic compound and metallic glass were carefully studied based on isothermal magnetization to reveal the exchange interactions in these two different structural stages, together with experimental electronic density analyses on the compound. Obtained critical exponents close to the theoretical values predicted by the mean-field theory (MFT) in both structures suggest the majority of Gd–Gd long-range exchange interactions, while the Co–Co direct interaction accounts for the deviation of these exponents from the theoretical values in MFT. This is likely a common feature for rare earth – transition metal ferrimagnets. The ordered Co atoms in the intermetallic compound exhibit a high-spin state ($\sim 4.6 \mu_B$), in contrast with the low-spin state of Co ($\sim 1.2 \mu_B$) in the metallic glass. The reduced spin is associated with the liquid-like structure in the metallic glass (e.g. longer Co–Co distances) and responsible for the low ordering temperature. This work also indicates that the substitution of p-block elements like Al prefers the site to diminish Co moments, leading to the significantly reduced ordering temperature, and thus emphasizes the critical role of d-electron elements to maintain enough direct exchange interactions for proper transition temperature in the development of new metallic glasses with giant magnetocaloric effects.

1. Introduction

With the rapid development of society and economy, environmental problems are becoming more and more serious, while one of the effective solutions is the eco-friendly technology. The motivation has led to huge advances in the research and development of new refrigeration technology based on the magnetocaloric effect (MCE), to avoid the release of Freon and CO_2 as well as the noise from the traditional mechanical refrigeration. Giant MCEs have been reported in several materials with first-order magnetic phase transitions (MPTs), e.g. La–Fe–Si

and $(Mn,Fe)_2(P,Si)$ series, but the hysteresis, narrow temperature span of MCEs and complicated preparation processes limit their application [1–5]. In contrast, materials based on second-order MPTs can depress these drawbacks, but their MCEs are generally smaller due to the absence of structural transitions. Thus large magnetic moments are necessary for materials of second-order MPTs to achieve large MCEs, and these materials are mainly based on heavy rare earth (RE) metals. Among them, Gd-based compounds attract more attention, due to their high ordering temperature close to room-temperature applications [6–9].

* Corresponding author.

** Corresponding author. School of Instrument Science and Opto-electronics Engineering & Institute of Quantum Sensing, Beihang University, Beijing, 100083, China.

E-mail addresses: gcsan@buaa.edu.cn (G. Shan), jiliangz@korea.ac.kr (J. Zhang).

<https://doi.org/10.1016/j.intermet.2020.106878>

Received 12 April 2020; Received in revised form 12 June 2020; Accepted 17 June 2020

Available online 30 June 2020

0966-9795/© 2020 Elsevier Ltd. All rights reserved.

Since the discovery of giant MCEs in $\text{Gd}_5\text{Si}_2\text{Ge}_2$ [6], many efforts are made to explore new Gd-based compounds and the doping on these compounds to improve their performance [7–10]. However, the number of Gd-based binary, ternary and quaternary compounds is limited, and some of them are even peritectic compounds. The doping into parent compounds also frequently leads to the secondary phase especially the congruent phases in the phase diagrams of Gd with dopants [11]. In contrast, Gd-based metallic glasses produced by quenching alloy melts provide an effective approach for continuously tuned compositions without a secondary phase even in binary systems [12–15]. Compared with their crystalline forms, the absence of crystal lattices will also depress the anisotropy in metallic glasses, and thus a sharper MPT is also expected in Gd-based metallic glasses, corresponding to larger MCEs [12–14]. Generally, a low melting temperature is necessary to produce metallic glasses, and thus the compositions of less than 1273 K in the melting temperature, especially those around eutectic points are ideal for the synthesis of metallic glasses [16]. According to binary phase diagrams [11], promising elements for Gd-based metallic glasses are mainly 3d transition metals (TMs) as well as some p-block elements, e.g. Mg and Al.

There are already many efforts on the MCEs of ternary and quaternary Gd-based Gd-Al-TMs metallic glasses with large glass-forming ability (GFA) [17,18]. As expected, these metallic glasses also show large MCEs generally estimated by large magnetic entropy change (ΔS) around their ordering temperatures (T_c) [17,18]. The ΔS of these metallic glasses are comparable to pure Gd and the well-known Gd-Si-Ge system [19,20]. However, the T_c of these metallic glasses is much lower compared with pure Gd and Gd-based compounds [6,19,21]. On the other hand, Gd-based Gd-TM binary metallic glasses show much higher T_c than those of multiple-component metallic glasses [14,15,17]. Although the Ruderman-Kittel-Kasuya-Yosida (RKKY) long-range interaction generally dominates the magnetism in RE-based materials with nonmagnetic elements including metallic glasses [22], the presence of TMs in these metallic glasses also implies the possible direct short-range interactions of Gd 5d – TM 3d electrons and TM 3d – TM 3d electrons, which are more important for a high T_c . Despite these possible strong direct exchange interactions, very few work are reported to understand such magnetic exchange interactions in these metallic glasses. A previous study on the critical behaviours of Si-doped Gd_4Co_3 metallic glasses has shown that the pristine Gd_4Co_3 is dominated by the 3D Heisenberg short-range interactions while the Si-doped is prevailed by the long-range exchange interactions [23]. This is in contradiction with the lower T_c of Gd_4Co_3 metallic glasses compared with the Si-doped Gd_4Co_3 and many Gd-based intermetallic compounds with long-range interactions [6–9]. In this work, we attempt to reveal the magnetic exchange interactions of $\text{Gd}_6\text{Co}_{4.85}$ metallic glasses from critical behaviours together with the $\text{Gd}_6\text{Co}_{4.85}$ intermetallic compound. The side-by-side study on the intermetallic compound and metallic glass deepens the understanding of exchange interactions especially direct interactions, while the experimental electronic structure of the $\text{Gd}_6\text{Co}_{4.85}$ compound supplies more hints on these magnetic exchange interactions for the tunable T_c .

2. Experimental

$\text{Gd}_6\text{Co}_{4.85}$ ingots were fabricated by arc melting the mixtures of pure constituent elements Gd (99.9 wt%, Alfa-Aesar) and Co (99.99 wt%, Alfa-Aesar) under a Ti-gettered argon atmosphere. Each alloy was remelted at least for three times to ensure the compositional homogeneity. Half of these ingots were sealed into quartz tubes under vacuum, which were then heated to 903 K at a ramping rate of 200 K/h and kept

for 2 weeks followed by air cooling to room temperature. Another half of these ingots were used to produce ribbon samples of metallic glasses (20 μm in thickness and 2 mm in width) by a single roller melt-spinning apparatus at a wheel surface speed of 40 m/s. The obtained ribbons have a shiny surface on the side next to the wheel, and a dark surface on the side opposite to the wheel. Phase identification was first performed on a Philips X'pert X-ray diffractometer with $\text{Cu K}\alpha$ radiation (1.5406 Å). The microstructure of polycrystalline ingots was examined using a JEOL 7400 F electron microscope equipped with an INCA-Oxford energy-dispersive spectrometer. Single crystals of the $\text{Gd}_6\text{Co}_{4.85}$ compound were selected from the annealed reaction products after breaking them and mounted on the top of glass fibers using Paratone N oil. Intensity data were collected at 100 K on a Bruker SMART CCD-diffractometer equipped with monochromated $\text{Mo K}\alpha$ radiation. The collected frames were then integrated and empirical absorption correction was made. The structures were refined on F^2 with the aid of the SHELXTL package [24]. The same refinements and crystallographic data were also reported in our previous work [25]. Here the refinement was used to extract structure factors. These structure factors were then used for the determination of electron density maps based on the maximum-entropy method (MEM) using the program Dysnomia [26], which maximizes the information theoretical entropy. The crystal structure and electronic density were visualized using VESTA [27]. The thermal stability of metallic glasses was measured with a PerkinElmer Diamond differential scanning calorimeter (DSC) at a heating rate of 40 K/min. Magnetization was measured using a physical properties measurement system (PPMS-9, Quantum Design Co.).

3. Scaling analysis

The secondary phase transition is a typical critical phenomenon, and thus the magnetization in vicinity can be well described using a scaling rule constructed by critical exponents, as detailed elsewhere. Briefly, the mathematical definitions of these critical exponents for magnetic systems can be expressed as follows [20]:

$$M_S(T) = M_0(-\epsilon)^\beta, \epsilon < 0 \quad (1)$$

$$\chi_0^{-1}(T) = \Gamma\epsilon^\gamma, \epsilon > 0 \quad (2)$$

$$M = DH^{1/\delta}, \epsilon = 0 \quad (3)$$

where:

$\epsilon = (T - T_c)/T_c$, the reduced temperature; H, the external magnetic field; M_0 , Γ , D, the critical amplitudes;

β , a critical exponent associated with the spontaneous magnetization M_S ;

γ , a critical exponent associated with the initial magnetic susceptibility χ_0 ;

δ , a critical exponent associated with the critical isothermal magnetization at T_c .

These exponents are actually not independent and can be correlated to yield a scaling hypothesis for the magnetic equation of state. According to the scaling hypothesis the magnetization can be expressed as:

$$M(H, \epsilon) = |\epsilon|^\beta f_\pm \left(\frac{H}{|\epsilon|^\beta + \gamma} \right) \quad (4)$$

where f_\pm are regular analytical functions with f_+ for $\epsilon > 0$, and f_- for $\epsilon < 0$. In terms of scaled magnetization $m \equiv |\epsilon|^{-\beta} M(H, \epsilon)$ and scaled field

$h \equiv |\varepsilon|^{-(\beta+\gamma)} H$, Eq. (4) can be written into the more familiar form:

$$m = f_{\pm}(h) \quad (5)$$

This equation implies that the scaled m plotted as a function of the scaled h will fall onto two different universal curves described by f_+ and f_- respectively, for true scaling relations and the right choice of these critical exponents.

These exponents generally show universal properties in the asymptotic region ($\varepsilon \rightarrow 0$), but various systemic trends or crossover phenomena are often observed, mostly due to the presence of various competing couplings and/or disorder. Therefore it is useful to introduce the temperature-dependent effective exponents for $\varepsilon \neq 0$, which are defined as [28]:

$$\beta_{\text{eff}}(\varepsilon) = \frac{d[\ln M_s(\varepsilon)]}{d(\ln \varepsilon)} \quad (6)$$

$$\gamma_{\text{eff}}(\varepsilon) = \frac{d[\ln \chi_0^{-1}(\varepsilon)]}{d(\ln \varepsilon)} \quad (7)$$

These effective exponents are general non-universal, but approach universal exponents in the asymptotic limit.

4. Results and discussions

4.1. Structure and magnetization

As shown in Fig. 1a, the powder X-ray diffraction (XRD) pattern of annealed ingots can be well indexed using the reported hexagonal structure in previous work ($\text{Gd}_6\text{Co}_{1.67}\text{Si}_3$ type, space group $P6_3/m$) [25], while the absence of Bragg reflections in XRD data of the ribbon samples confirms their glassy nature. The grain sizes of the intermetallic compound vary from less than 20 μm to more than 70 μm , and no obvious impurity is observed despite several cavities (see the inset in Fig. 1a). The thermal analysis on the metallic glasses shows strong endothermic peaks for crystallization which can be deconvoluted into three endothermic peaks as seen in Fig. 1b, while the signal for glass transition is very weak (see the inset in Fig. 1b) compared with the ternary Gd-Co-Al metallic glasses of high glass-forming ability (GFA) [29]. The onset and peak temperatures of the deconvoluted peaks for crystallization are listed in Table 1. The multiple peaks of crystallization especially the

Table 1

Characteristic temperatures of deconvoluted peaks in DSC curves of the $\text{Gd}_6\text{Co}_{4.85}$ metallic glass.

Peak	1	2	3
T_{onset} (K)	574.4(5)	585.5(5)	610.2(5)
T_{peak} (K)	582.8(5)	595.0(5)	627.3(5)

overlap between the first crystallization peak and the main peak may suggest two different kinds of crystal structures formed from the $\text{Gd}_6\text{Co}_{4.85}$ metallic glasses. In another word, the same composition cannot lead to homogeneous nucleation of the counterpart compound. It is not unexpected, because the solidification curve of the $\text{Gd}_6\text{Co}_{4.85}$ melt also shows two close exothermic peaks for crystallization [25]. The determined glass transition temperature T_g is 542.0(6) K, much lower than the values close to 600 K in Gd-based ternary and quaternary bulk metallic glasses with high GFA [13,17]. The estimated supercooled temperature region ($\Delta T = T_{\text{onset}} - T_g$) is around 32 K and smaller than the nearly 50 K in Gd-based bulk metallic glasses [13,17], suggestive of the relatively low GFA. The low GFA also accounts for the weak signal for glass transition in the DSC data.

Despite the same composition, the temperature dependent magnetization shows that the $\text{Gd}_6\text{Co}_{4.85}$ intermetallic compound has a higher T_c than the metallic glass (220(1) K against 210(1) K). The high-temperature paramagnetic region in both crystal and glassy samples can be well described using the Curie-Weiss law [29], $\chi(T) = C/(T - \theta)$, where $C = N_A \mu_{\text{eff}}^2 / 3k_B$ is the Curie constant, N_A Avogadro number, k_B Boltzmann constant, μ_{eff} effective magnetic moment and θ the paramagnetic Curie temperature. When the temperature is close to the ordering temperature, an evident deviation from the linear relationship is evident in the crystalline compound, while the deviation in the metallic glass is much smaller. The hyperbolic in the data of reciprocal susceptibility just above T_c is a typical feature in ferrimagnetic systems, which can be described using a Néel-type relationship [30]:

$$\frac{1}{\chi} = \frac{1}{\chi_0} + \frac{T}{C} - \frac{\sigma}{T - \theta} \quad (8)$$

where χ_0 is temperature-independence susceptibility, σ is related to the molecular field coefficients. The value of Curie constant C in the equation is deduced from the asymptotic region of the hyperbola and

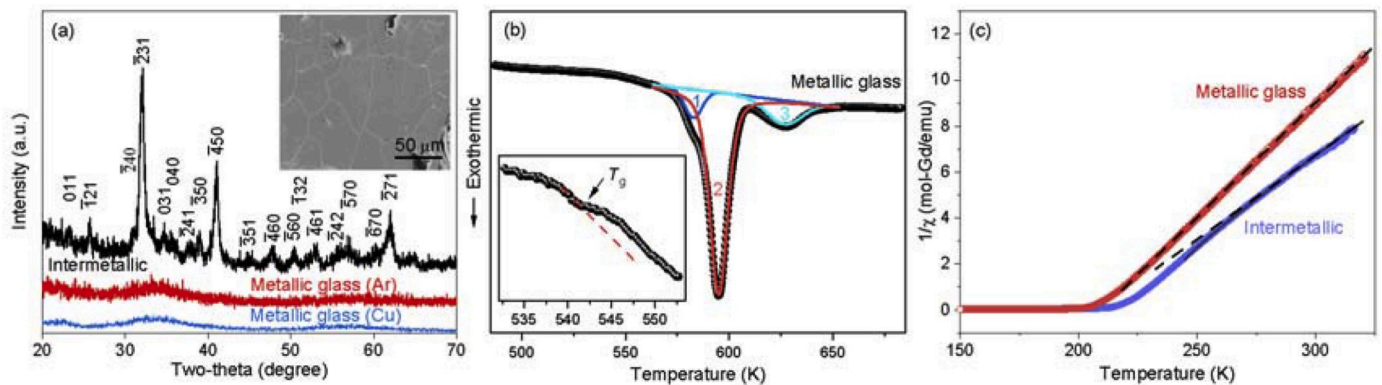


Fig. 1. (Color online, double column) XRD patterns (a), thermal analysis (b) and temperature dependent magnetization (c) of the $\text{Gd}_6\text{Co}_{4.85}$ intermetallic compound and metallic glasses. The inset in (a) presents the microstructure of the intermetallic compound, and the inset in (b) shows how the glass transition is determined. Miller indexes label well the XRD reflections of crystalline samples in (a), and the red and blue patterns correspond to the dark and shiny sides of the glassy ribbon respectively. The color lines in (b) show three deconvoluted peaks of the crystallization process in the metallic glass, and the dashed line in the inset is to emphasize the glass transition. Dash lines in (c) represent the Curie-Weiss fitting, while the solid line is for the Néel-type relationship.

thus is the same as that obtained from the linear regression of Curie-Weiss law. Generally, C' obtained by the fit is larger than the real Curie constant, due to the thermal variation of the molecular field coefficients [30], while the real Curie constant can be corrected as [31]:

$$\frac{1}{C} = \frac{1}{C'} - \frac{\gamma}{\chi_0} \quad (9)$$

where γ is a characteristic constant of the system. Here $\gamma = 4 \times 10^{-4}$ (for Gd_6Co_3) was adopted [32], and the estimated effective moments μ_{eff} using the corrected Curie constant are $10.2 \mu_B$ per Gd atom for the crystal compound and $8.9 \mu_B$ per Gd atom for the metallic glass. Both values are larger than the theoretical value of free Gd ($7.94 \mu_B$), suggestive of the extra contribution from Co for Gd-Co ferrimagnetic couplings. However, the different Co contribution in two kinds of structures implies different magnetic exchange interactions. To inspect such difference, analysis on the critical behaviors around T_c was performed.

4.2. Critical behaviors

According to the Landau theory, the free energy G of a magnetic system can be expanded in the powers of its order parameter M near the transition, expressed as [33]:

$$G(T, M) = G_0 + \frac{1}{2}A(T)M^2 + \frac{1}{4}B(T)M^4 + \dots - MH \quad (10)$$

where A and B are temperature-dependent coefficients, and the last term describes the energy of spins in an external field H . The higher order items are generally negligible in practice. The energy is minimized ($\frac{\partial G}{\partial M} = 0$) at equilibrium, According to the mean-field theory, the magnetic equation of states at equilibrium can be expressed in the form of Arrott formula [34]:

$$\frac{M}{H} = A + BM^2 \quad (11)$$

Therefore the M^2 versus H/M curves should be straight lines, and the intercept on the H/M axis determines the ordering transition. However, this approach does not take into account the microscopic exchange interactions and fluctuations in magnetic systems. Therefore critical exponents are introduced into a modified Arrott (MA) formula to include these short-range and direct interactions, as [35]:

$$\left(\frac{M}{H}\right)^{1/\gamma} = A\varepsilon + BM^{1/\beta} \quad (12)$$

Critical exponents β and γ predicted by mean-field, 3D-Ising and 3D-

Table 2

Comparison of critical exponents of two different $\text{Gd}_6\text{Co}_{4.85}$ structures with typical Gd-based intermetallic compounds and theoretical models.

composition	Technique	β	γ	Ref.
$\text{Gd}_6\text{Co}_{4.85}$ (intermetallic)	Modified Arrott Plot	0.538 (1)	1.078(1)	present
	Kouvel-Fisher method	0.538 (1)	1.078(2)	present
$\text{Gd}_6\text{Co}_{4.85}$ (glass)	Modified Arrott Plot	0.495 (2)	1.065(6)	present
	Kouvel-Fisher method	0.498 (1)	1.052(4)	present
Gd_5Si_4	Modified Arrott Plot	0.48		[38]
$\text{Gd}_5\text{Si}_2\text{Ge}_2$	Modified Arrott Plot	0.56		[38]
Gd_6FeBi_2	Modified Arrott Plot	0.441 (8)	1.098 (12)	[21]
	Kouvel-Fisher method	0.446 (6)	1.092 (10)	[21]
3D Ising		0.325	1.241	[36]
3D Heisenberg		0.365	1.386	[36]
Mean Field		0.5	1	[34]

Heisenberg models are listed in Table 2 [34,36]. Nevertheless, a real magnetic system is generally more complex than predicted by these models, and thus the critical parameters may be different from values for these models.

To determine critical exponents in Eq. (12) for the present systems, a Python code was developed based on the following procedures: First, with any initial values between those predicted by the means-field model and the 3D-Ising or Heisenberg models, the linear extrapolation of the high field portions of the isotherms will give an intercept on both $M^{1/\beta}$ and $\left(\frac{M}{H}\right)^{1/\gamma}$ axis, from which the spontaneous magnetization M_S and the inverse initial susceptibility χ_0^{-1} can be calculated. By Eqs. (3) and (4), these calculated data will generate new critical exponents. The best values of β and γ obtained should be self-consistent with the values yielded by fitting Eq. (12). Previous work shows that effective exponents converge approaching to the universal exponents only when $\varepsilon < 0.1$ [36]. Thus only the data in this range are employed to estimate critical exponents. After several cycles, the exponents finally converge into stable values (see Appendix). The values obtained after 150 cycles are $\beta = 0.538(3)$, $\gamma = 1.078(2)$ for the intermetallic compound and $\beta = 0.495(18)$, $\gamma = 1.065(6)$ for the metallic glass. Evidently, MA plots of both the compound and the metallic glass exhibit good linearity around T_c as shown in Fig. 2. The spontaneous magnetization M_S and the inverse initial susceptibility χ_0^{-1} obtained using these exponents are then plotted

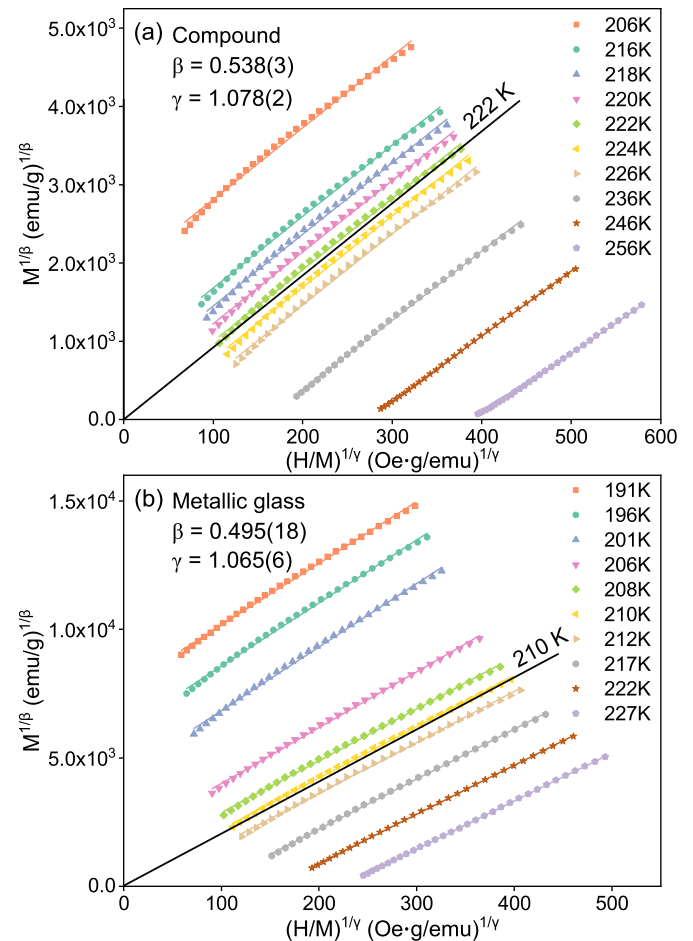


Fig. 2. (Color online, single column) Modified Arrott plots using optimized critical components for the $\text{Gd}_6\text{Co}_{4.85}$ intermetallic compound (a) and metallic glass (b).

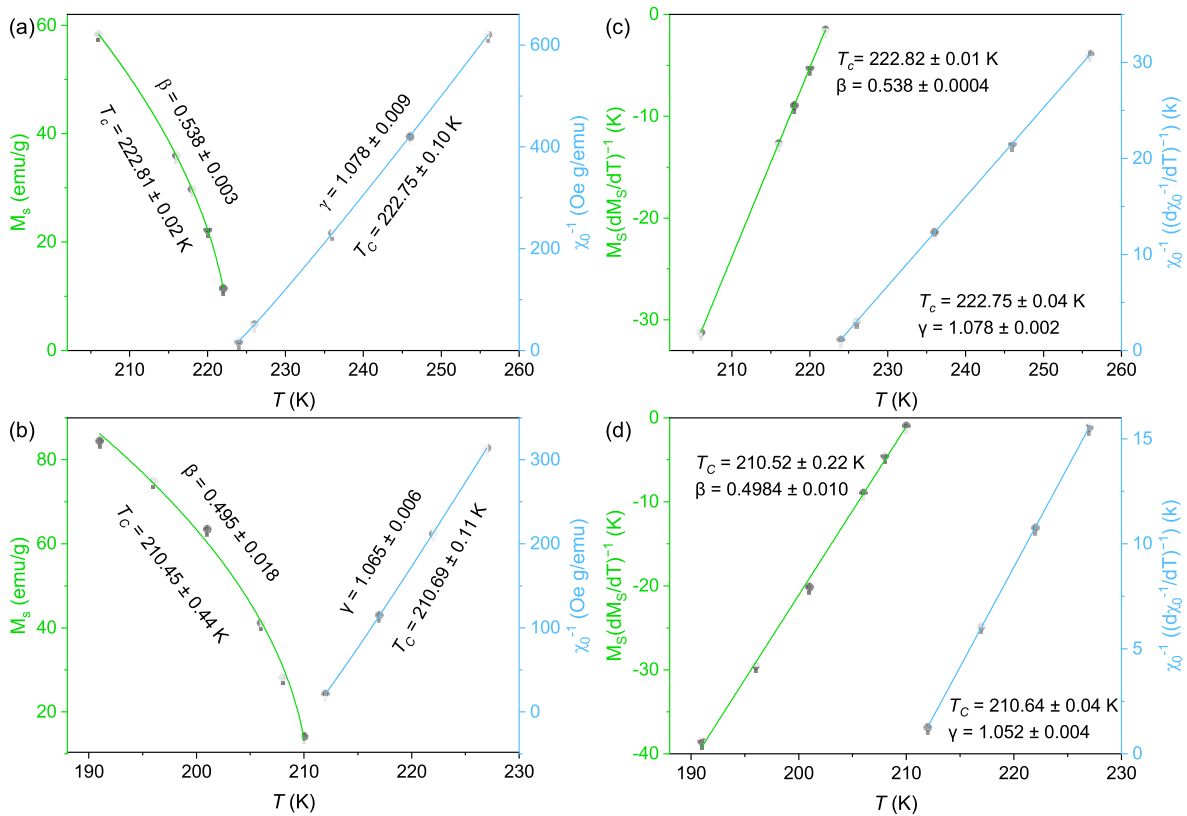


Fig. 3. (Color online, double column) Temperature variation in spontaneous magnetization $M_s(T)$ (left axis) and inverse initial susceptibility $\chi_0^{-1}(T)$ (right axis) for the compound (a) and metallic glass (b), as well as Kouvel-Fisher plot of spontaneous magnetization $M_s(T)$ (left axis) and inverse initial susceptibility $\chi_0^{-1}(T)$ (right axis) for the compound (c) and metallic glass (d). Solid lines in (a) and (b) are guides for eyes, and straight lines in (c) and (d) are due to linear fitting of data.

as a function of temperature in Fig. 3a and b. The fitting of these values to Eq. (3) gives $\beta = 0.538(3)$, $T_c = 222.81(2)$ K, and to Eq. (4) gives $\gamma = 1.078(2)$, $T_c = 222.75(10)$ K for the $\text{Gd}_6\text{Co}_{4.85}$ compound. The corresponding values for the metallic glass are $\beta = 0.495(18)$, $T_c = 210.45(44)$ K, $\gamma = 1.065(6)$, $T_c = 210.69(11)$ K. These values are also listed in Table 2 for comparison. Obviously, these values in both structures are close to those given by the mean-field model rather than the 3D-Ising or 3D-Heisenberg model. Compared with the compound, the critical exponents closer to values predicted by the mean-field model in the metallic glass suggest less magnetic contribution from short-range exchange interactions, in good agreement with the results of the temperature dependent magnetization in Fig. 1c.

Except for above method, another approach, the Kouvel-Fisher (KF) method [37] can also be used to determine the critical exponents and T_c more precisely, which is expressed as:

$$M_s \left(\frac{dM_s}{dT} \right)^{-1} = (T - T_c) / \beta \quad (13)$$

$$\chi_0^{-1} \left(\frac{d\chi_0^{-1}}{dT} \right)^{-1} = (T - T_c) / \gamma \quad (14)$$

In this method, the straight lines in plots of $M_s \left(\frac{dM_s}{dT} \right)^{-1}$ vs. T and $\chi_0^{-1} \left(\frac{d\chi_0^{-1}}{dT} \right)^{-1}$ vs. T yield slopes $1/\beta$ and $1/\gamma$ in critical regions respectively, and intercepts of such fitted straight lines on their T axis equal to T_c . Thus this method requires no previous knowledge of T_c and provides

a consistency condition for T_c , namely, the fitting of both plots should give the same value of T_c . Using determined M_s and χ_0^{-1} by MA plots (Fig. 3a and b), the KF plots of two structures are shown in Fig. 3c and d, and estimated critical exponents and T_c by fitting these straight lines are: $\beta = 0.538(1)$, $T_c = 222.8(1)$ K and $\gamma = 1.078(2)$, $T_c = 222.8(1)$ K for the compound; $\beta = 0.498(10)$, $T_c = 210.5(2)$ K and $\gamma = 1.052(4)$, $T_c = 210.6(1)$ K for the metallic glass. These values are very typical for Gd-based intermetallic compounds [21,38], e.g. Gd_5Si_4 , $\text{Gd}_5\text{Si}_2\text{Ge}_2$ and Gd_6FeBi_2 , as listed in Table 2. If a magnetic impurity described by Eq. (3) was treated as a paramagnetic state corresponding to Eq. (4) by mistake, a large γ is expected, because χ is proportional to M and thus apparent γ in the mistake is proportional to the inverse β . It accounts for the observed critical exponents close to the values for 3D Ising or Heisenberg model in the Gd-based ferrimagnets, which are dominated by long-range exchange interactions actually.

All these critical exponents estimated from above methods match reasonably well, suggestive of their self-consistency, as tabulated in Table 2. To confirm whether these critical exponents follow the scaling equation of state, the plots of scaled m against scaled h is drawn using the values in Table 2, which depicts the two different universal curves distinctly in both structures as predicted by the scaling equation Eq. (7) (Fig. 4). The same plots on the log-log scale as inset in Fig. 4, also clearly suggest the converging of two curves towards T_c . Both plots confirm the reliability of these critical exponents and T_c .

4.3. Electronic structures and exchange interactions

The analysis of critical behaviors shows the dominant long-range

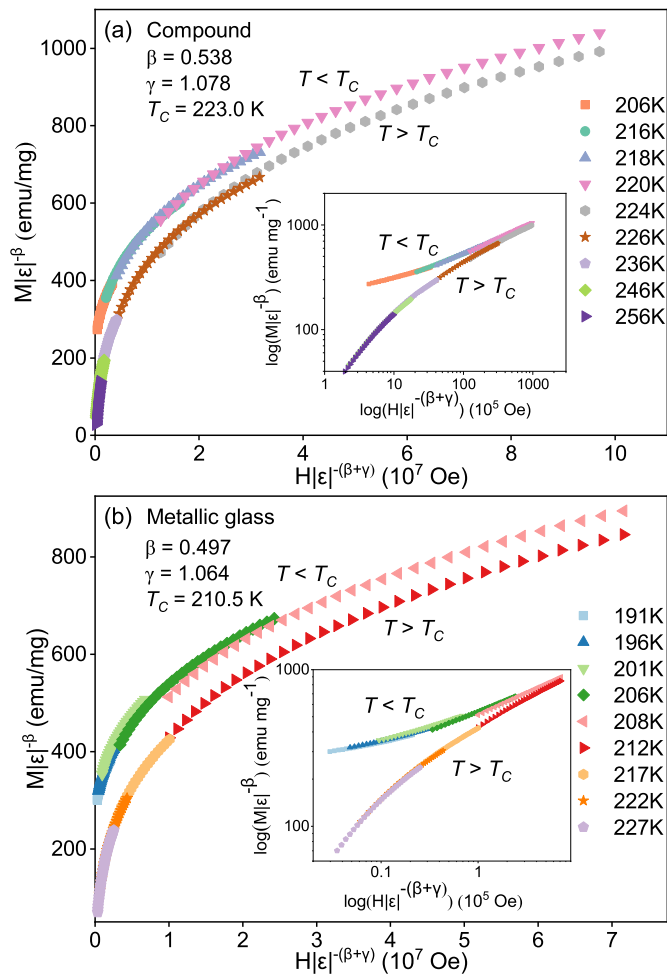


Fig. 4. (Color online, single column) Scaled magnetization of the $\text{Gd}_6\text{Co}_{4.85}$ compound (a) and metallic glass (b) below and above T_C , using critical exponents given by the Kouvel-Fisher plot. The insets show the same plot on a log-log scale.

exchange interactions in both structure, while the temperature dependent magnetization also suggests the significant role of short-range interaction from Co likely via Co-Co contacts, which seems to be the major difference corresponding to their different magnetic performance. It is difficult to figure out the exact atomic structure in the metallic glass for the analysis of Co-Co interaction, but the analysis on the compound

may also supply information on these exchange interactions based on the above side-by-side comparison.

The intermetallic compound adopts the $\text{Gd}_6\text{Co}_{1.67}\text{Si}_3$ -type structure, and the crystal structure is schematically shown in Fig. 5a. Gd atoms occupy two different 6h (Gd1 and Gd2) sites, and Co atoms take two ordered sites (2c for Co1, 6h for Co2) and two disordered 4e sites. For TMs like Fe and Co, the low spin state is generally favored for free atoms energetically, and this is also the case of many compounds with low TM concentration. In these compounds, the TM atom is isolated by non-magnetic or RE atoms and thus show no magnetic moment due to the dilute effect of surrounding atoms, like in RE_6CoTe_2 [39]. In the present compound, disordered Co atoms are well isolated by Gd1 atoms, and likely show no magnetic contribution as observed in $\text{Gd}_6\text{Co}_{1.67}\text{Si}_3$ [40]. In contrast, the close Co-Co contact in ordered Co atoms enables a strong overlap of the 3d electron wave functions of neighboring atoms to form 3d electron bands where the relatively strong effective Coulomb repulsion between 3d electrons can favour even large unequal numbers of spin-up and spin-down electrons resulting in the high spin state.

To confirm this inference, MEM analysis was employed to optimize the electron density based on structure factors from single-crystal XRD data collected at 100 K. The difference electron density was obtained by the subtraction of the electron density calculated using the spherical approximation of these atoms. The crystal phase (001) at $z = 0.75$ was chosen for the analysis, as shown in Fig. 5b. The Co1 atom centered in the Co2 triangle shows clearly an anisotropic valence electron distribution with high electron density towards three neighboring Co2 atoms. Similarly, the valence electron distribution of all three Co2 atoms also significantly elongated towards Co1, suggestive of the strong direct interaction between Co1 and Co2. The strong interaction corresponds to the large overlap of the 3d electron wave functions of Co1 and Co2, accounting for the high spin state. Nevertheless, the difference electron density distribution of the disordered Co atoms is more isotropic and less affected by the surrounding Gd atoms. Thus the overlap between the Co 3d electron wave functions and valence electrons of Gd atoms should be very small, favoring the low spin state in disordered Co atoms. Compared with ordered Co atoms, the distribution of valence electrons in Gd atoms is more uniform (see the blue zone around nuclei in Fig. 5b). The effective moment of $10.2 \mu_B$ per Gd atom estimated from the temperature dependent magnetization (Fig. 1c) suggests an extra moment of Co as $2.8 \mu_B$ per Co atom on average in the compound, close to the theoretical value of the intermediate spin ($2.83 \mu_B$). As discussed above, the disordered Co atoms show no magnetic contribution, and thus one ordered Co atom will carry a large effective moment of ca. $4.6 \mu_B$, corresponding to the value of high spin ($4.9 \mu_B$) [41].

The estimated effective moment of Co in the metallic glass is $1.2 \mu_B$ per atom on average, much smaller than that in the compound. Because

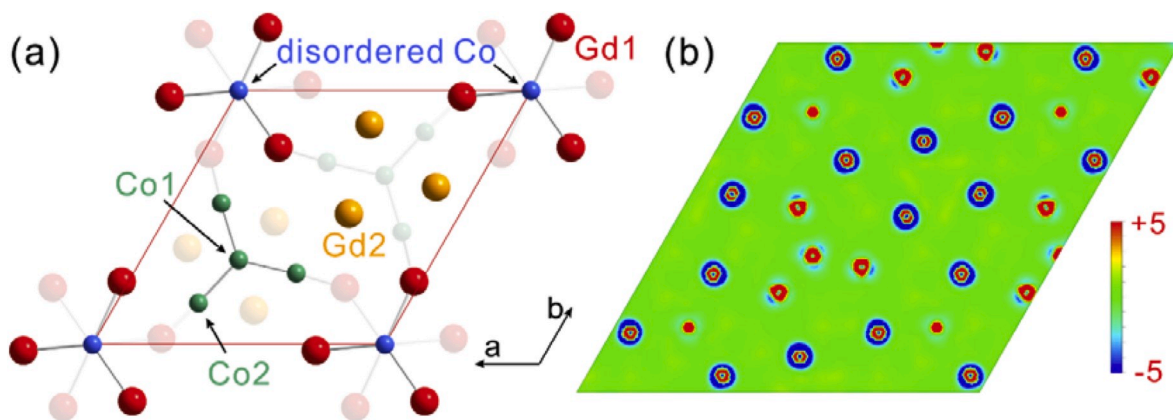


Fig. 5. (Color online, 1.5 column) Represent crystal structure of the $\text{Gd}_6\text{Co}_{4.85}$ intermetallic compound viewed along c axis, and the difference electron density map projected on the same (001) crystal plane ($z = 0.75$). The shallow atoms in (a) are in the parallel crystal plane ($z = 0.25$) next to the top plane. The red frame in (a) shows the unit cell. The unit in the legend for difference electron density is e/a_0^3 where a_0 is the Bohr radius.

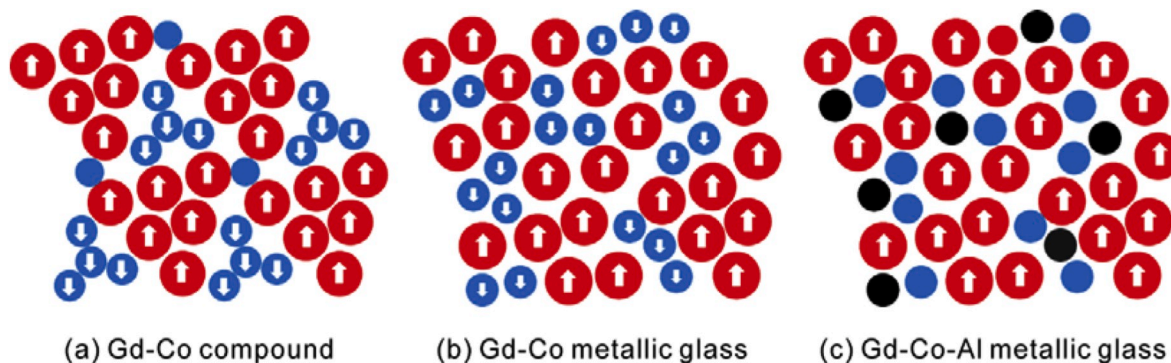


Fig. 6. (Color online, double column) Schematic illustration on the atomic structure and magnetic interactions in Gd-rich Gd-Co compound (a), metallic glass (b) and Gd-Co-Al metallic glasses (c). The arrows illustrate the net spin of Co and Gd as well as their exchange interactions. Red cycles are for Gd, blue for Co and black for Al.

the metallic glass is regarded as the frozen alloy melt, the atomic distribution should be more homogenous unlike two significantly different kinds of Co atoms in the compound. Compared with the high spin state, the dramatically reduced Co moment in the metallic glass is not surprised, because the longer Co-Co distance in the frozen glassy structure will lead to a small overlap of 3d electron wave function between two neighboring Co atoms, favoring the lower spin.

Despite the small fraction of Co-Co exchange interactions in these Gd-based materials, the Co 3d – Co 3d exchange coupling is much stronger than the long-range indirect interactions between Gd atoms, due to the localized Co 3d electrons compared with the dispersed Gd 6s electrons. The exchange energy for Gd is around 25 meV [22], while the energy for Co is more than 100 meV depending on the spin state [42]. Thus the direct exchange interaction of these 3d electrons plays a more critical role for a high T_c , as characterized by the ferrimagnetic feature above T_c in Fig. 1c. In this view, it is important to maintain the Co-Co direct interaction in metallic glasses to achieve a desirable temperature for magnetic refrigeration.

According to the above discussion, the variation of atomic structure and magnetic interactions from the $Gd_6Co_{4.85}$ intermetallic compound to the $Gd_6Co_{4.85}$ metallic glass and to the Gd-Co-Al metallic glasses can be schematically illustrated in Fig. 6. The ferrimagnetic ground state with antiparallel couples between Co spins and Gd spins leads to the net magnetic moment from Gd, and thus the net magnetization can be described using by critical exponents close to values given by the mean-field theory for the long-range interaction. Compared with the Gd sublattice, the high-spin Co can maintain the magnetic ordering at a higher temperature in the $Gd_6Co_{4.85}$ intermetallic compound (Fig. 6a). In the glassy structure, the Co spin is reduced but the number of magnetic Co increases (Fig. 6b), so that the T_c is only slightly lower than that of the intermetallic compound. Actually, the T_c of this binary metallic glass is already much higher than those of Gd-Co-Al metallic glasses, e.g. 124 K for $Gd_{60}Co_{25}Al_{15}$ [43] and 95 K for $Gd_{55}Co_{17.5}Al_{17.5}$ [44]. Obviously, the spin in Co should be significantly depressed or Co may even show no magnetic contribution in these Gd-Co-Al metallic glasses, suggesting that Al prefers the sites to isolate Co in these metallic glasses (Fig. 6c). In this regard, d-electron elements are better candidates for doping or substitution in Gd-based metallic glasses to keep a high T_c during the exploration on new materials for magnetic refrigeration.

5. Conclusions

The side-by-side study of the $Gd_6Co_{4.85}$ intermetallic compound and metallic glass was performed on their critical behaviours to reveal the exchange interactions in them, especially the direct interactions of Co. Both structures have a ferrimagnetic ground state, whose net magnetization is from Gd and close to the model given by the mean-field theory. In contrast, the Co-Co direct interactions in two structure are very different: ordered Co atoms in the intermetallic compound show a high-spin state ($4.6 \mu_B$) accompanied with nonmagnetic Co at disordered sites, which is also supported by the MEM analysis of electron density, while the Co atoms in the metallic glass carry much lower spins ($1.2 \mu_B$). These direct interactions play dominant roles on the high T_c in these materials. The reduced spin in the metallic glass is associated with the liquid-like structure, e.g. longer Co-Co distance and small numbers of Co-Co contact. According to this investigation, the substitution of p-block elements like Al prefers the sites to diminish Co moments and leads to the significantly reduced T_c in Gd-Co-Al metallic glass. Therefore the work presented here emphasizes the critical role of d-electron elements to preserve direct exchange interactions for the development of high- T_c metallic glasses with giant MCE.

Declaration of competing interest

The authors declare that they have no known competing financial interests or personal relationships that could have appeared to influence the work reported in this paper.

CRediT authorship contribution statement

Guoming Cui: Formal analysis, Writing - original draft. **Xin Li:** Writing - original draft, Formal analysis. **Guangcun Shan:** Supervision, Validation, Writing - review & editing. **Haibin Gao:** Formal analysis. **Kam Wa Wong:** Formal analysis. **Jiliang Zhang:** Conceptualization, Supervision, Writing - original draft, Writing - review & editing.

Acknowledgments

This work was supported by the National Key R&D Program of China (Grant No. 2016YFE0204200) and the Fund of Advanced Innovation Center of Big Data Precision Medicine of Beihang University.

Appendix. Convergence tests of the fitting on Modified Arrott plots using Python code

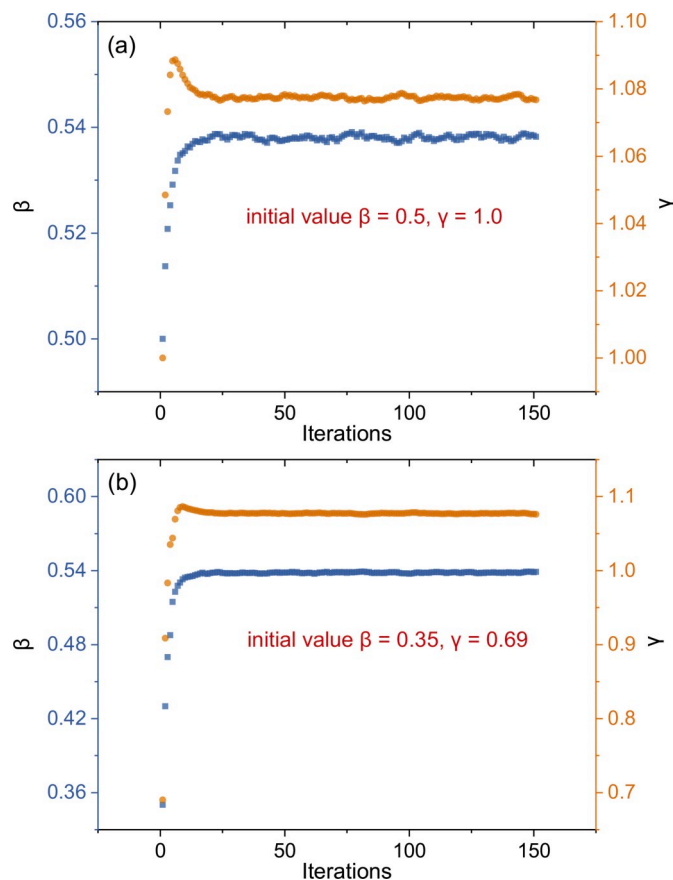


Fig. A1. Convergence of the fitting on Modified Arrott plots of the $Gd_6Co_{4.85}$ intermetallic compound using different initial values for critical exponents in the Python codes. The code is available on request.

References

- [1] T. Gottschall, D. Benke, M. Fries, A. Taubel, I.A. Radulov, K.P. Skokov, O. Gutfleisch, A matter of size and stress: understanding the first-order transition in materials for solid-state refrigeration, *Adv. Funct. Mater.* 27 (2017) 6, <https://doi.org/10.1002/adfm.201606735>.
- [2] L.M. Moreno-Ramirez, C. Romero-Muniz, J.Y. Law, V. Franco, A. Conde, I. A. Radulov, F. Maccari, K.P. Skokov, O. Gutfleisch, Tunable first order transition in $La(Fe,Cr,Si)_{13}$ compounds: retaining magnetocaloric response despite a magnetic moment reduction, *Acta Mater.* 175 (2019) 406–414, <https://doi.org/10.1016/j.actamat.2019.06.022>.
- [3] A. He, V. Svitlyk, Y. Mozharivskiy, Synthetic approach for $(Mn,Fe)_2(Si,P)$ magnetocaloric materials: purity, structural, magnetic, and magnetocaloric properties, *Inorg. Chem.* 56 (2017) 2827–2833, <https://doi.org/10.1021/acs.inorgchem.6b02912>.
- [4] O. Tegus, E. Bruck, K.H.J. Buschow, F.R. de Boer, Transition-metal-based magnetic refrigerants for room-temperature applications, *Nature* 415 (2002) 150–152, <https://doi.org/10.1038/415150a>.
- [5] F. Guillou, A.K. Pathak, D. Paudyal, Y. Mudryk, F. Wilhelm, A. Rogalev, V. K. Pecharsky, Non-hysteretic first-order phase transition with large latent heat and giant low-field magnetocaloric effect, *Nat. Commun.* 9 (2018) 9, <https://doi.org/10.1038/s41467-018-05268-4>.
- [6] V.K. Pecharsky, K.A. Gschneidner, Giant magnetocaloric effect in $Gd_5(Si_2Ge_2)$, *Phys. Rev. Lett.* 78 (1997) 4494–4497, <https://doi.org/10.1103/PhysRevLett.78.4494>.
- [7] F. Eustermann, F. Stegemann, M. Radziejowski, O. Janka, Intermetallic $RE_6T_5Al_7$ phases ($RE = Sc, Y, Ce-Nd, Sm, Gd-Lu; T = Ru, Ir$): diversity in their magnetic, magnetocaloric, and critical properties, *Inorg. Chem.* 58 (2019) 16211–16226, <https://doi.org/10.1021/acs.inorgchem.9b02732>.
- [8] J. Zhang, J.-J. Lee, T. Yang, W. He, Y.-M. Kang, S. Bobev, Tunable magnetic exchange between rare-earth metal 5d and iron 3d states: a case study of the multiple magnetic transitions in Gd_6FeBi_2 and the solid solutions $Dy_{6-x}Gd_xFeBi_2$ ($1 \leq x \leq 5$) with Curie temperatures in the range 120–350 K, *Chem. Mater.* 32 (7) (2020) 3087–3096, <https://doi.org/10.1021/acs.chemmater.0c00060>, online.
- [9] J. Zhang, G. Shan, Z. Zheng, C.H. Shek, Structure and magnetic behaviors of Gd_6FeBi_2 compound, *Intermetallics* 68 (2016) 51–56, <https://doi.org/10.1016/j.intermet.2015.07.013>.
- [10] J. Zhang, Y.-M. Kang, G. Shan, S. Bobev, Structural analysis of Gd_6FeBi_2 from single-crystal X-ray diffraction methods and electronic structure calculations, *Acta Crystallogr. C* 75 (2019) 562–567, <https://doi.org/10.1107/S2053229619004868>.
- [11] T.B. Massalski, *Binary Alloys Phase Diagrams*, ASM International, Materials Park, OH, 1990.
- [12] M.N. Song, L.W. Huang, B.Z. Tang, D. Ding, X. Wang, L. Xia, Enhanced Curie temperature and magnetic entropy change of $Gd_{63}Ni_{37}$ amorphous alloy by Co substitution, *Intermetallics* 115 (2019) 106614, <https://doi.org/10.1016/j.intermet.2019.106614>.
- [13] L. Xue, J. Li, W.M. Yang, C.C. Yuan, B.L. Shen, Effect of Fe substitution on magnetocaloric effects and glass-forming ability in Gd-based metallic glasses, *Intermetallics* 93 (2018) 67–71, <https://doi.org/10.1016/j.intermet.2017.11.007>.
- [14] C. Wu, D. Ding, L. Xia, K.C. Chan, Achieving tailorable magneto-caloric effect in the Gd-Co binary amorphous alloys, *AIP Adv.* 6 (2016), 035302, <https://doi.org/10.1063/1.4943506>.
- [15] J.L. Zhang, Z.G. Zheng, W.H. Cao, C.H. Shek, Magnetic behavior of Gd_4Co_3 metallic glass, *J. Magn. Magn. Mater.* 326 (2013) 157–161, <https://doi.org/10.1016/j.jmmm.2012.09.002>.
- [16] Y. Li, Bulk metallic glasses: eutectic coupled zone and amorphous formation, *JOM* 57 (2005) 60–63, <https://doi.org/10.1007/s11837-005-0236-5>.
- [17] Q. Luo, W.H. Wang, Magnetocaloric effect in rare earth-based bulk metallic glasses, *J. Alloys Compd.* 495 (2010) 209–216, <https://doi.org/10.1016/j.jallcom.2010.01.125>.
- [18] C. Wu, D. Ding, L. Xia, Effect of Al addition on the glass-forming ability and magnetic properties of a Gd-Co binary amorphous alloy, *Chin. Phys. Lett.* 33 (2016), 016102, <https://doi.org/10.1088/0256-307X/33/1/016102>.
- [19] A.M. Tishin, Magnetocaloric effect in lanthanide materials, *J. Alloys Compd.* 250 (1997) 635–641, [https://doi.org/10.1016/S0925-8388\(96\)02521-2](https://doi.org/10.1016/S0925-8388(96)02521-2).
- [20] V. Provenzano, A.J. Shapiro, R.D. Shull, Reduction of hysteresis losses in the magnetic refrigerant $Gd_5Ge_2Si_2$ by the addition of iron, *Nature* 429 (2004) 853–857, <https://doi.org/10.1038/nature02657>.

- [21] G. Cui, H. Ma, K.W. Wong, C.H. Shek, G. Shan, J. Zhang, Understanding high ordering temperature in Gd_6FeBi_2 magnet: critical behavior, electronic structure and crystal-field analysis, *J. Magn. Magn Mater.* 499 (2020) 166301, <https://doi.org/10.1016/j.jmmm.2019.166301>.
- [22] K.A.J.E. Gschneidner L, *Handbook on the Physics and Chemistry of Rare Earth*, Elsevier, Amsterdam, 1979.
- [23] Z.G. Zheng, X.C. Zhong, Z.W. Liu, D.C. Zeng, V. Franco, J.L. Zhang, Magnetocaloric effect and critical behavior of amorphous $(Gd_4Co_3)_{1-x}Si_x$ alloys, *J. Magn. Magn Mater.* 343 (2013) 184–188, <https://doi.org/10.1016/j.jmmm.2013.04.087>.
- [24] SHELXTL, Bruker AXS Inc., Madison, WI, 2003.
- [25] J. Zhang, Z. Zheng, G. Shan, S. Bobev, C.H. Shek, Abnormal thermal expansion, multiple transitions, magnetocaloric effect, and electronic structure of $Gd_6Co_{4.85}$, *J. Appl. Phys.* 118 (2015) 133903, <https://doi.org/10.1063/1.4931982>.
- [26] K. Momma, T. Ikeda, A.A. Belik, F. Izumi, Dysnomia, a computer program for maximum-entropy method (MEM) analysis and its performance in the MEM-based pattern fitting, *Powder Diffr.* 28 (2013) 184–193, <https://doi.org/10.1017/S088571561300002X>.
- [27] K. Momma, F. Izumi, VESTA: a three-dimensional visualization system for electronic and structural analysis, *J. Appl. Crystallogr.* 41 (2008) 653–658, <https://doi.org/10.1107/S0021889808012016>.
- [28] H.E. Stanley, *Introduction to Phase Transitions and Critical Phenomena*, Oxford University Press, London, 1971.
- [29] L. Shao, L. Xue, Q. Luo, Q. Wang, B. Shen, The role of Co/Al ratio in glass-forming GdCoAl magnetocaloric metallic glasses, *Materialia* 7 (2019) 100419, <https://doi.org/10.1016/j.mtla.2019.100419>.
- [30] J.S. Smart, *Effective Field Theories of Magnetism*, Saunders, Philadelphia, PA, 1966.
- [31] L. Néel, Antiferromagnetism and ferrimagnetism, *Proc. Phys. Soc.* 65 (1952) 869–885, <https://doi.org/10.1088/0370-1298/65/11/301>.
- [32] J.S. Smart, The Néel theory of ferrimagnetism, *Am. J. Phys.* 23 (1955) 356–370, <https://doi.org/10.1119/1.1934006>.
- [33] E. Burzo, Paramagnetic behavior of some rare-earth cobalt compounds, *Phys. Rev. B* 6 (1972) 2882–2887, <https://doi.org/10.1103/PhysRevB.6.2882>.
- [34] L.P. Levy, *Magnetism and Superconductivity*, Springer-Verlag, Berlin Heidelberg, 2000.
- [35] A. Arrott, Criterion for ferromagnetism from observations of magnetic isotherms, *Phys. Rev.* 108 (1957) 1394–1396, <https://doi.org/10.1103/PhysRev.108.1394>.
- [36] A. Arrott, J.E. Noakes, Approximate equation of state for nickel near its critical temperature, *Phys. Rev. Lett.* 19 (1967) 786–789, <https://doi.org/10.1103/PhysRevLett.19.786>.
- [37] S.N. Kaul, Static critical phenomena in ferromagnets with quenched disorder, *J. Magn. Magn Mater.* 53 (1985) 5–53, [https://doi.org/10.1016/0304-8853\(85\)90128-3](https://doi.org/10.1016/0304-8853(85)90128-3).
- [38] J.S. Kouvel, M.E. Fisher, Detailed magnetic behavior of nickel near its Curie point, *Phys. Rev.* 136 (1964) A1626–A1632, <https://doi.org/10.1103/PhysRev.136.A1626>.
- [39] J.H. Belo, A.M. Pereira, C. Magen, L. Morellon, M.R. Ibarra, P.A. Algarabel, J. P. Araújo, Critical magnetic behavior of magnetocaloric materials with the Gd_5Si_4 -type structure, *J. Appl. Phys.* 113 (2013) 133909, <https://doi.org/10.1063/1.4798578>.
- [40] A.V. Morozkin, Y. Mozharivskiy, V. Svitlyk, R. Nirmala, O. Isnard, P. Manfrinetti, A. Provino, C. Ritter, Magnetic properties of Fe_2P -type R_6CoTe_2 compounds ($R=Gd-Er$), *J. Solid State Chem.* 183 (2010) 1314–1325, <https://doi.org/10.1016/j.jssc.2010.04.002>.
- [41] E. Gaudin, S. Tence, F. Weill, J.R. Fernandez, B. Chevalier, Structural and magnetocaloric properties of the new ternary silicides $Gd_6M_{5/3}Si_3$ with $M=Co$ and Ni , *Chem. Mater.* 20 (2008) 2972–2979, <https://doi.org/10.1021/cm8000859>.
- [42] N.N. Lubinskii, L.A. Bashkurov, A.I. Galyas, S.V. Shevchenko, G.S. Petrov, I. M. Sirota, Magnetic susceptibility and effective magnetic moment of the Nd^{3+} and Co^{3+} ions in $NdCo_{1-x}Ga_xO_3$, *Inorg. Mater.* 44 (2008) 1015–1021, <https://doi.org/10.1134/S0020168508090197>.
- [43] E.P. Wohlfarth, *Handbook of Magnetic Materials*, North Holland, Amsterdam, 1980.
- [44] H. Fu, M. Zou, Magnetic and magnetocaloric properties of ternary Gd–Co–Al bulk metallic glasses, *J. Alloys Compd.* 509 (2011) 4613–4616, <https://doi.org/10.1016/j.jallcom.2011.01.126>.